Interaction of H2/O2 flames with inert walls

Francois DABIREAU and Bénédicte CUENOT,
CERFACS, Toulouse

Olivier VERMOREL
IMFT, Toulouse

and

Thierry POINSOT
CERFACS & IMFT, Toulouse

Full-length article

Corresponding author:
Dr. B. Cuenot
CERFACS
42 A. G. Coriolis
31057 Toulouse cedex 1
France

Tel 33 5 61 19 30 44
Fax 33 5 61 19 30 00

email: cuenot@cerfacs.fr

Numerical simulations of the interaction of an H2-O2 flame and a wall are performed. Two situations are considered: a premixed flame propagating towards the wall and a diffusion flame staying at a distance from the wall. In both cases chemical processes controlling the interaction are studied in detail. The thermal fluxes to the wall are evaluated and the maximal value, as well as the interaction duration, are compared. Results show that the premixed flame leads to high fluxes to the wall, during a short time before quenching. The diffusion flame leads to lower values for the maximum flux, but high flux levels are maintained for a longer time. Finally the total energy transferred to the wall is comparable for both flames.

1 Introduction

The mechanisms occuring in the near-wall regions of combustion chambers control essential aspects of engine performances: the maximum wall heat fluxes and the formation of unburnt hydrocarbons for example, are often due to flames interacting with walls ([1], [2], [3], [4]). Most flame - wall studies have been performed for hydrocarbon fuels-air premixed flames. However hydrogen combustion has gained interest in the last few years because of its applications in the aerospace domain, where new emerging techniques require a perfect knowledge of near-wall combustion phenomena and wall transfers. Flame - wall interaction (FWI) has been studied in premixed flames theoretically ([1]), experimentally ([2],[3]) and numerically for both laminar ([4], [6]) and turbulent flows ([7], [8]). FWI studies for turbulent premixed flames suggest that simple estimates may be found for maximum wall fluxes ([4], [7]): typically, the maximum heat flux observed in a premixed combustion chamber is the flux Φ_Q^p measured in laminar flames.
Two generic FWI cases in laminar flows must be considered (Fig. 1), depending on the flame front orientation to the wall. When the flame front is parallel to the wall, the configuration is called head-on quenching (HOQ); when it is perpendicular to the wall, the configuration is called side-wall quenching (SWQ). Both situations may occur for premixed and diffusion flames. However the mechanisms are quite different for the two types of flames.
Premixed flames in the HOQ configuration quench at a certain distance of the wall y_Q (of the order of

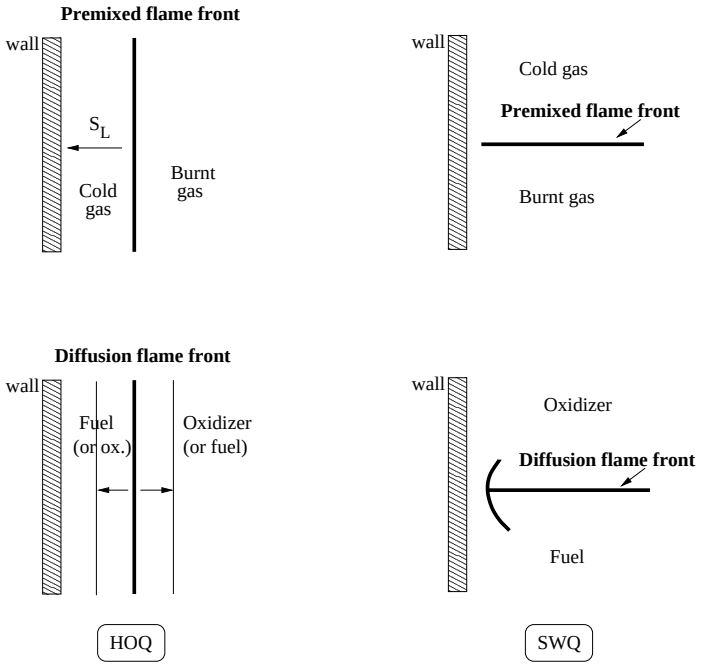

Figure 1: The basic configurations for flame-wall interaction.

the flame thickness). For a planar flame, this interaction is one-dimensional and unsteady. The wall flux Φ_Q is maximum when the flame quenches. For hydrocarbon/air flames, typical values of Φ_Q^p are about one third of the total flame power ([6]). In the SWQ configuration, premixed flames stabilize at a quenching distance y_Q of the wall, generally larger than for HOQ, leading to slightly lower wall fluxes. This situation can be described in terms of a two-dimensional stationary problem.
Although FWI is rather well understood in premixed flames, much less work has been devoted to diffusion flames. For such flames, even identifying the generic FWI configurations is a difficult task.

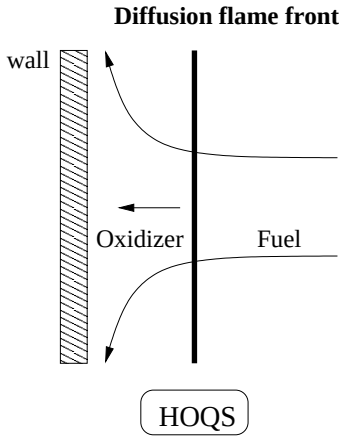

Figure 2: The head-on quenching with strain (HOQS) configuration for the diffusion flame.

The main difference between HOQ for premixed and diffusion flames is that the diffusion flame does not propagate: it remains close to its initial position, at a fixed distance y from the wall. The reactants and the hot products diffuse towards both sides of the flame, reach the wall and interact with it. In this case the initial flame position is an added free parameter of the problem definition, compared to the premixed flame HOQ. A better defined configuration may be the head-on quenching with strain (HOQS) configuration (Fig. 2), in which the diffusion flame is placed in a counter-flow that controls its thickness through the constant strain rate Λ and pushes the flame towards the wall. Recent DNS ([5]) have shown that this configuration could lead to large fluxes: maximum heat fluxes for such HOQS cases can be twice as large as the flux caused by the HOQ of a stoichiometric premixed flame under the same thermodynamic conditions. Finally side wall quenching (SWQ) may also be observed for diffusion flames. The diffusion flame edges interacting with the wall may have a complex structure (propagating triple flames) and this case will be presented in another paper.

We present here a detailed numerical study of H2/O2 premixed and diffusion flame HOQ, considering complex chemistry and transport properties. The chemical processes involved in the interaction, the wall heat flux histories and the interaction mechanisms are studied in detail. The obtained maximum wall heat flux, interaction duration and total exchanged energy are compared for both flames.

2 HOQ flame-wall interaction for a premixed flame

Previous studies have shown that a single step model is unable to correctly predict quenching phenomena, especially at high wall temperature, i.e. $T_w > 400$K [3]. Single step mechanisms tend to overestimate the wall heat flux due to the absence of low activation energy recombination reactions in the near-wall region. In order to give a detailed insight into the complex mecanisms of flame-wall interaction, a 8-species, 18-reactions scheme stemming from [9] was used here.

For an inert wall, and neglecting the radiative heat transfer, the wall heat flux is given by $\Phi = \lambda_w(\partial T/\partial x)_w$ where λ_w is the thermal conductivity of the mixture at the wall. Using the laminar flame power of the unstrained flame, $q_l^0 = \rho_u Y_{F,u} S_l^0 \Delta H$ as a reference value, where Y_F is the fuel mass fraction, s_L^0 is the unstretched laminar flame speed and ΔH is the heat produced by the flame, Φ is normalized to obtain the non-dimensional wall heat flux $\phi = \Phi/q_l^0$ (here a subscript u denotes unburnt gas and b burnt gas). We are mostly interested by the maximum non-dimensional wall heat

flux during the flame-wall interaction, denoted ϕ_Q.
Due to complex chemistry, there is no single and univoque definition of the flame position. Indeed, the position of the flame may be located either at the maximum heat release $\dot{\omega}_{max}$ or at the maximum fuel reaction rate $\dot{\omega}_{F,max}$, which are generally different. The corresponding flame-wall distances will be noted $y_{\dot{\omega}_{max}}$ and $y_{\dot{\omega}_{F,max}}$ respectively. The quenching distances will be denoted by the subscript "$_Q$". Most authors normalize these distances by a characteristic flame thickness $\delta = \lambda_u/(\rho_u C_p s_L^0)$, that yields to the Peclet numbers, $Pe = y_{\dot{\omega}_{max}}/\delta$ and $Pe_F = y_{\dot{\omega}_{F,max}}/\delta$ respectively. The flame thickness is defined as $\delta_L^0 = \Delta T/(\partial T/\partial x)_{max}$ ($\delta_L^{0*} = \delta_L^0/\delta$ for the non-dimensional form), where $\Delta T = T_b - T_u$. One can also define a characteristic time of the interaction: t_Q, as the time interval corresponding to the heat flux increase from $\phi_Q/2$ to ϕ_Q. This time is non-dimensionalized by the characteristic flame time $t_F = \delta/s_L^0$, so that $t_Q^* = t_Q/t_F$.

Numerical method

The whole set of the compressible one-dimensional multi-species reacting flows equations is solved using a sixth-order finite difference scheme in space combinated with a third-order Runge-Kutta scheme in time. Cross-diffusional effects (Soret and Dufour effects) are taken into account. Chemistry is described using a detailed kinetic scheme, taken from [9]. Catalytic reactions at the wall are not included in the kinetic model. Fluid properties, molecular transport coefficients and reaction source terms are computed using CHEMKIN [10] and TRANSPORT [11].
Before the flame-wall interaction calculations are started, a steady one-dimensional laminar premixed flame is calculated using PREMIX [12]. The calculations are initialized with this flame, placed far enough from the wall. A boundary condition of inert isothermal wall is imposed at the left-hand side of the computational domain using the NSCBC method [13]. The temperature of the wall is kept constant at $T_w = T_u = 750$K where T_u is the unburned gas temperature. This implies that there is no thermal boundary layer. Indeed, for pressures near the atmospheric pressure, it is known that the boundary layer does not significantly affect the heat transfer [14]. On the right-hand side of the domain, a non-reflecting boundary condition is used.

Results and diagnostics

For a H2/O2 stoichiometric mixture at 1 bar and 750K, PREMIX calculations give the burnt gas temperature $T_b = 3130$K, the laminar flame speed $s_L^0 = 3197$ cm/s and the characteristic flame thickness $\delta = 1.2\ \ 10^{-3}$ cm. The total fuel reaction rate, defined by $\dot{\omega}_{F,tot} = \int_{-\infty}^{+\infty} \dot{\omega}_F dx$, is equal in this case to $q_l^0/\Delta H$.
The time evolutions of the non-dimensional characteristic parameters of the flame-wall interaction (Pe, Pe_F, ϕ, δ_L^{0*} and non-dimensional total fuel reaction rate $\dot{\omega}_{F,tot}^* = \dot{\omega}_{F,tot}/(q_l^0/\Delta H)$) are plotted in Fig. 3. t^* is the non-dimensional time $t^* = t/t_F$.

This head-on-quenching process may be split up into three distinct stages.

- In the first stage, the flame propagates at a constant speed equal to the laminar flame speed. All the species, temperature and heat release profiles are identical to those of the equivalent undisturbed flame. The non-dimensional flame thickness δ_L^{0*} is of the order of 25. In front of the flame, in the induction zone, the stable species H_2 reacts with radical species to produce H atoms. The main reactions for H_2 consumption are: $H_2 + OH \rightarrow H_2O + H$ (R1) and $O + H_2 \rightarrow OH + H$

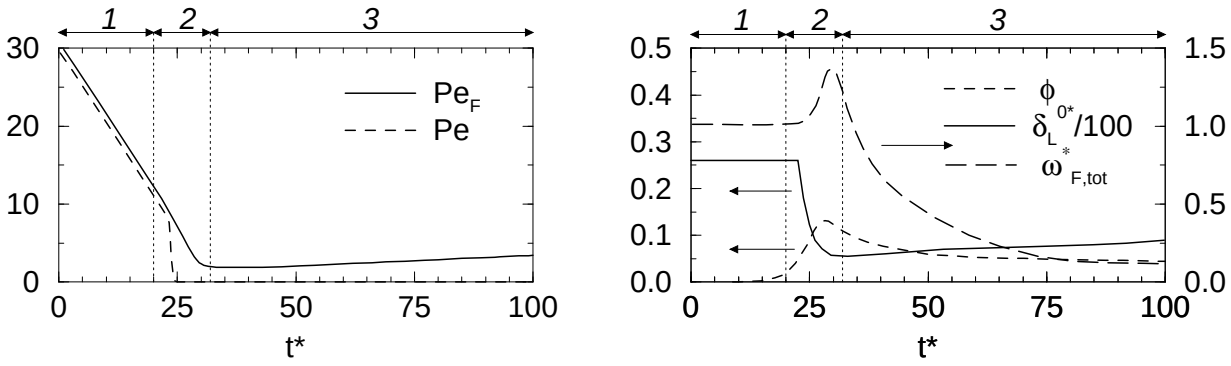

Figure 3: Non-dimensional characteristic parameters of the flame-wall interaction.

(R2). Then, these H atoms are oxidized in the reaction zone producing other radical species. In this zone, the main part of the heat of reaction is released. Far from the wall, these radical species diffuse from the reaction zone to the induction zone to pre-oxidize H_2. This propagation phase lasts from $t^* = 0$ to $t^* = 20$.

- In the second stage, the flame still move towards the wall but begins to feel the presence of the wall. It corresponds to Peclet numbers $Pe = 10.7$ and $Pe_F = 12.1$. The flame-wall interaction starts with a slight increase in the total reaction rate about $t^* = 20$. It is followed by a sharp drop in the flame thickness around $t^* = 23$. At that time, the wall heat flux has a value of about 25% of its maximum value. At $t^* = 24$, the peak value of heat release reaches the wall ($Pe = 0$) while the increase in the total reaction rate is still very low. The maximum reduced wall heat flux $\phi_Q = 0.129$ is obtained at a reduced time $t^* = 29$. Nevertheless, the total fuel reaction rate keeps on increasing until $t^* = 30$ to reach a value equal to 1.33 time the reference value of the free propagating flame. The flame slows down but still propagates. It is finally quenched around $t^* = 32$ ($Pe_{F,Q} = 1.7$) when the flame thickness is at its lowest value. Mechanims occurring during what we called this second stage are well known and identical whatever the fuel is (see [15] for exemple).

  As before, H_2 is mainly pre-oxidized thanks to radical species OH and O. These radical species can also be consumed by recombination to produce stable species via reaction $H + OH + M \rightarrow H_2O + M$ (R3) in particular. However, reaction rates of these recombination reactions are negligible if the induction zone temperature is high. This is what happens when the flame is far from the wall, i.e. when the induction zone temperature is high enough. When the wall gets closer, thermal losses induced by the wall make the induction zone temperature decrease. Then, reaction rates of H_2 pre-oxidization reactions decrease whereas reaction rates of recombination reactions increase preventing H_2 from being decomposed. The consumption speed of the flame reduces then up to the quenching of the flame at a distance $Pe_{F,Q}$ from the wall.

- The third stage of the flame-wall interaction starts then. The total reaction rate and the wall heat flux decrease slowly to zero but the combustion is not completed yet. Indeed, H_2 molecules which have not been consumed diffuse now towards the hot burned gas where radical species concentration is high to allow its post-oxidization. This is the reason why Pe_F increases after $t^* = 32$. Of particular interest is the fact that all these mechanisms seem to remain unchanged in a large range of pressure and equivalence ratio.

The interaction characteristic parameters ($\phi_Q = 0.129$, $Pe_{F,Q} = 1.7$ and $t^*_Q = 4.69$), appear to be notably different from those obtained in hydrocarbon-air flames (see [16] and [14] for example). The main difference concerns the non-dimensional wall heat flux ϕ_Q: many studies present values equal to one-third approximately whereas we obtain only 0.129. Dimensional results also show a particular behavior of H2/O2 flames, with very high wall heat fluxes. These high wall heat fluxes, combined with short interaction times, prove that the H2/O2 flame-wall interaction is very intense and very fast compared to the hydrocarbon-air flames. This is due first to the components nature (H2/O2 flames are very exothermic and rapid flames) and, second, to the choice of a high wall temperature since the wall heat flux is known to increase with increasing wall temperature [3]. Another reason is that, due to the fast diffusion of the species, a H2/O2 flame goes very close to the wall, much closer than a hydrocarbon-air flame.

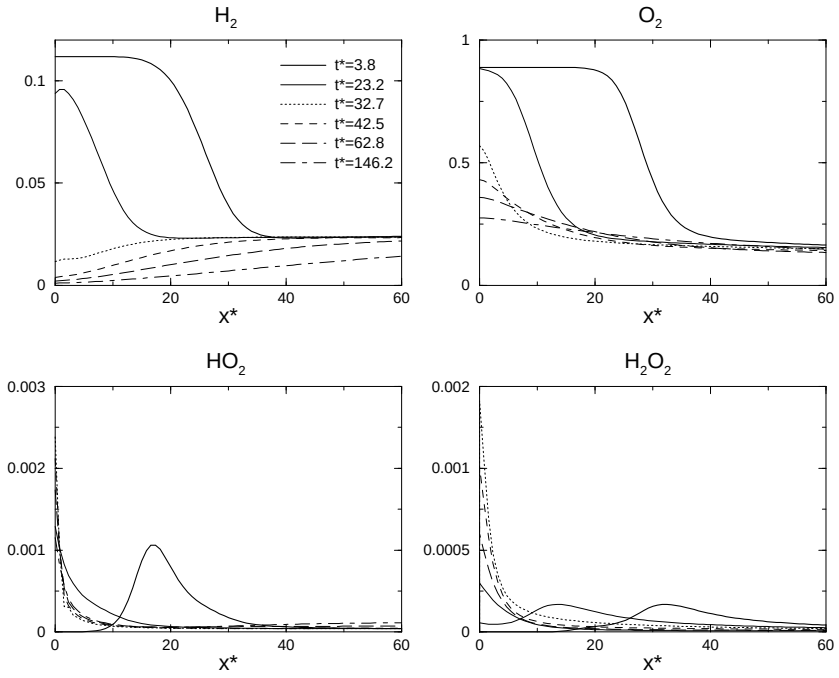

Figure 4: Mass fraction profiles.

In Fig. 4, mass fraction profiles of species H_2, O_2, HO_2 and H_2O_2 are plotted as functions of the non-dimensional distance from the wall $x^* = x/\delta$ at six different non-dimensional times t^*. All the profiles for $t^* < 20$ are similar to undisturbed flame profiles: the peak values and the shape of the mass fraction fields remain unchanged, which means that the flame has not yet entered the influence zone of the wall. Then, from $t^* = 20$ and until the quenching time $t^* = 29$, the main feature is the accumulation of species HO_2 and H_2O_2 directly at the wall. This phenomenon is particularly striking for the stable intermediate species H_2O_2 since its peak value is multiplied by 7 compared to its value in the free propagating flame. It is important to note that the first species to accumulate at the wall is HO_2. Indeed, in the free propagating flame, the main HO_2 production zone is located ahead of the induction zone, placing the peak value of HO_2 concentration closest to the wall when the flame approaches it. Moreover, HO_2 may be produced in the low temperature near wall region through reactions $H + O_2 + M \rightarrow HO_2 + M$ (R4) and $H + 2O_2 \rightarrow HO_2 + O_2$ (R5) because of their low activation energies. Since the temperature is relatively low in this region, the only way to consume

HO_2 is via the low activation energy recombination reaction $HO_2 \rightarrow H_2O_2 + O_2$ (R6). This explains the high concentration of H_2O_2 at the wall and the low decrease of O_2 concentration compared to H_2, although the mixture is in stoichiometric proportions. This reaction is exothermic and results in a high heat release directly at the wall. This remarkable process is difficult to predict. Indeed, HO_2 and H_2O_2 have very low concentrations in the free flame (about 10^{-3} for HO_2 and 10^{-4} for H_2O_2) and do not seem to play a crucial role there. The presence of the wall completely changes the kinetic mechanism and makes it necessary to have a good description of these two species, though it strongly raises computing times. Calculations without HO_2 and H_2O_2 have shown a reduction by 30% of the maximum wall heat flux, independently of the pressure or the equivalence ratio.
The profiles of the radical species O, H and OH remain almost the same as in the free propagating flame, with the same peak values, until flame quenching. These radical species do not have maximum concentrations at the wall because the temperature there is not high enough to allow chain branching reactions to proceed. After $t^* \approx 29$, all profiles become flat because of the species diffusion from the near-wall cold region to the burned gas hot region. H_2 and H, having the lowest molecular weight are the fastest to diffuse and are finally post-oxidized in the hot gas.

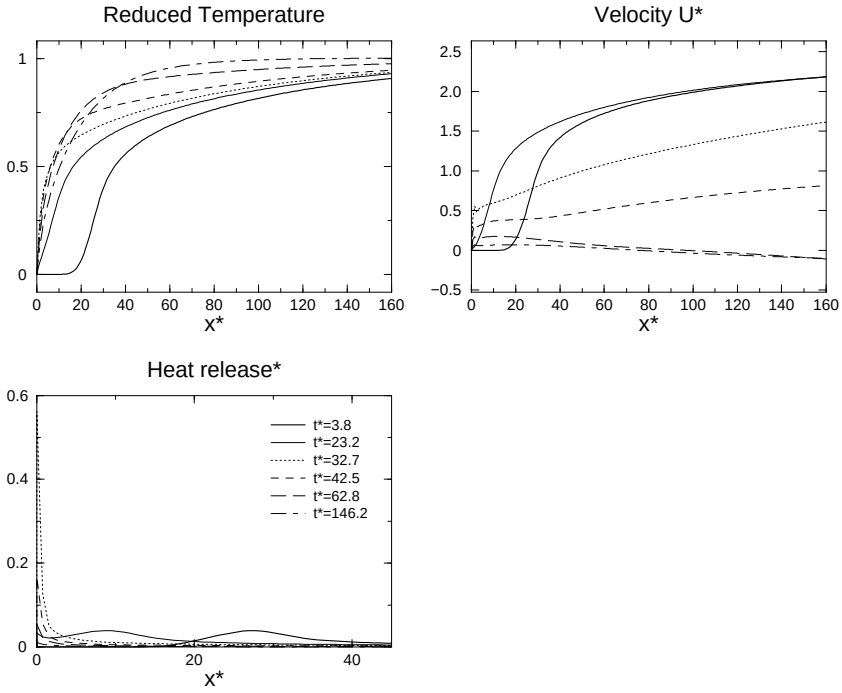

Figure 5: Non-dimensional heat release, temperature and velocity profiles.

Fig. 5 displays the profiles of the non-dimensional heat release $\dot{\omega}^*_T = \dot{\omega}_T/(q_l^0/\delta)$, the reduced temperature $T^* = (T - T_u)/(T_b - T_u)$ and the non-dimensional gas velocity $u^* = u/s_L^0$, at the same times as in the previous figure. They confirm the scenario previously described. The velocity and temperature profiles show again that, until about $t^* = 20$, the flame does not see the wall and propagates like a free flame. Then the velocity decreases gradually to become negative at the time of the post-oxidization, while the temperature profile experiences an important stiffening at the wall. The flame thickness decreases by 80% during the flame-wall interaction, leading to an increase of the maximum temperature gradient by a factor of approximately 5. This points out that a very refined mesh is necessary in the near wall region. This becomes a delicate problem when decreasing the wall

temperature, as this means an even greater temperature gradient increase.
The heat release profile shows a very similar behavior to the H_2O_2 one. This suggests that this species could serve as good marker of the region of maximum heat release in the flame. The fact that the peak value of heat release is directly at the wall is characteristic of a high wall temperature condition. This is confirmed by several studies that have related the lower wall temperature condition to a peak value of heat release located further away from the wall. Here, it is important to mention that catalytic reactions are not included in the kinetic model. Calculations in [17] for a methane-air flame show that a reactive wall assumption leads to smaller heat release rate and radical concentration at the wall, as radical adsorption reactions are added to radical recombination reactions. However, it is concluded that these phenomena are especially important for the free radicals H and OH. In our calculations, the concentrations of these species are very low at the wall, and one may consider that catalysis effects are negligible.

3 HOQ flame-wall interaction for a diffusion flame

The HOQ diffusion flame-wall interaction configuration is similar to the premixed flame case. Besides the flame structure, the main difference between HOQ premixed or diffusion flame-wall interaction is that the premixed flame propagates towards the wall whereas the diffusion flame stays close to its initial position.This initial position is an added free parameter of the problem definition compared to the premixed flame case and will be discussed. Moreover in diffusion flames, two different situations exist, depending on wether $H2$ or $O2$ is trapped between the flame and the wall. It is known that having $O2$ near the wall leads to higher wall heat fluxes ($H2$ is generally used to protect chamber walls), and this configuration was retained here.

Numerical Method

The flow and the boundary conditions are the same as for the premixed flame. Calculations are initialized by placing at a distance y from the wall a steady strained H2/O2 diffusion flame previously calculated with OPPDIFF [10]. When the computation starts, the initial velocity field is set to zero: the flame is not strained anymore and diffuses. Here the flame position is identified by the location of maximum temperature T_b. The initial flame-wall distance is chosen so as to reach the maximum possible flux, i.e. to place the flame as close as possible to the wall without perturbing it (see Fig. 6). Dioxygen is placed at the left-hand side of the domain at a temperature $T_{O_2} = T_w = 750$K whereas dihydrogen is located at the right-hand side at an initial temperature $T_{H_2} = 300$K.

The almost steady position of the diffusion flame makes the initial flame-wall distance a key point of the resulting wall heat flux. Considering that the wall heat flux is directly linked to the ratio $\Delta T/y$ with $\Delta T = T_b - T_w$ (cf. [18]), it is reasonable to say that a minimum distance y corresponds to a maximum wall heat flux. This minimum distance is directly linked to the flame thickness, itself related to the strain rate of the flame Λ (see Fig. 7). When the initial flame strain rate increases, the initial flame thickness decreases and the flame may be placed closer to the wall without being perturbed. Assuming that a strain rate variation does not imply a significant variation of the flame maximum temperature T_b, the maximum wall heat flux reached during head-on-quenching of a diffusion flame is expected for a minimum initial flame thickness, i.e. for a strain rate close to the critical extinction strain rate.

The objective is first to study the maximum wall heat flux as a function of the initial distance y

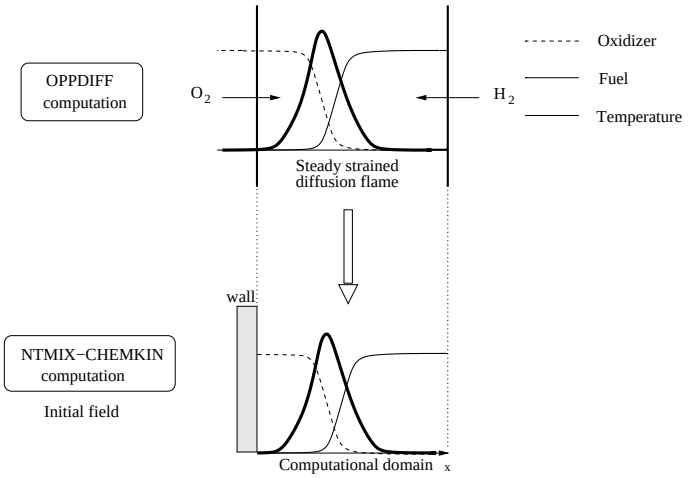

Figure 6: Initialisation of diffusion flame-wall interaction.

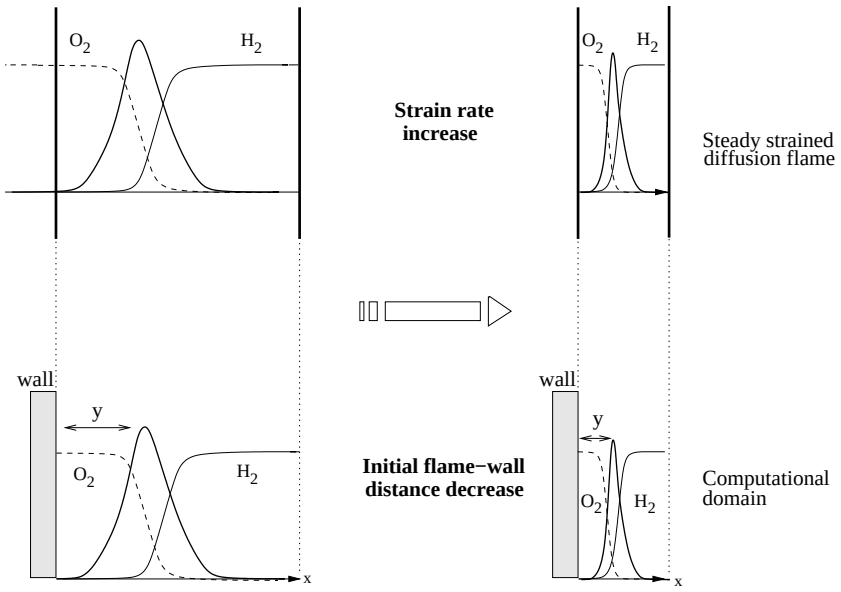

Figure 7: Determination of initial flame-wall distance as a function of the strain rate.

for a fixed initial strain rate Λ. Next, different strain rates are used to obtain the maximum wall heat flux in a H.O.Q. situation of a diffusion flame.
For the first calculations series, the initial strain rate Λ is $6300s^{-1}$, a low value compared to the extinction strain rate $\Lambda_Q = 235000s^{-1}$. This allows to minimize the mesh requirements and save computing time.

Results and diagnostics

Calculations have been made for four different non-dimensional distances $y^* = y/\delta$. To allow comparison, all non-dimensional variables are calculated with the same reference values as in the premixed

flame case.
In a first stage, the flame moves slightly back due to the velocity field induced by the flame. However this induced field is low and decreases rapidly to zero. Then the flame position becomes steady and lateral diffusion starts. Little by little, intermediate species accumulate directly at the wall. Like in the premixed case, HO_2 and H_2O_2, which peak farthest on the oxidizer side, are the first species to reach the wall. However, for the diffusion flame, these concentrations remain relatively low. This is due to two effects. First HO_2 and H_2O_2 concentrations are initially lower in the diffusion flame than in the premixed flame. Second, the H atoms required by the formation of HO_2 via low activation recombination reactions (R4) and (R5) are mainly concentrated on the fuel side and not close to the wall. Consequently, peak values of heat release remain in the high temperature region, i.e. at a finite distance to the wall. An illustration of this phenomenon can be seen in Fig. 8 where non-dimensional heat release profiles are displayed at six distinct times $t^* = t/t_F$ and for an initial distance $y^* = 87.1$. This value corresponds to an initial flame thickness of approximately 160 times δ, i.e. 6 times δ_L^0.

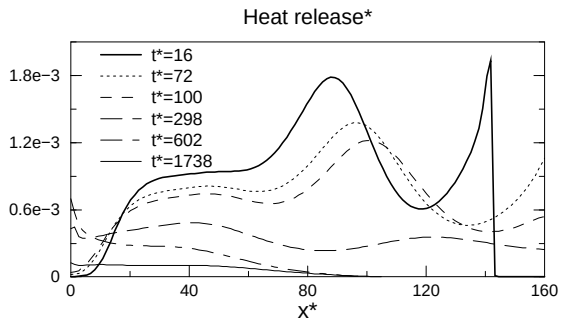

Figure 8: Non-dimensional heat release profiles for $y^* = 87.1$.

Although the mechanisms including HO_2 and H_2O_2 species seem to be less important in the interaction process in the case of a diffusion flame, calculations show that the contribution of HO_2 and H_20_2 species to the wall heat flux is still about 30%, i.e. of the same order of magnitude as in a premixed flame. This would be probably wrong if the reactant trapped between the wall and the flame was H_2, since HO_2 and H_2O_2 are almost non-existent on the fuel side.
The peak value of the reduced heat release $\dot{\omega}_T^*$ reaches the wall at a time $t^* = 320$ only, i.e. right in the middle of the interaction process whereas, for the premixed flame, it is observed at the beginning (i.e. at the beginning of the "second stage"). The maximum wall heat flux is reached at the time $t^* = 602$. At this time, the heat release is almost equal to zero in the whole domain except in the near-wall region.
Fig. 9 compares the time evolution of the non-dimensional wall heat flux ϕ and the reduced total heat release $\dot{\omega}_{T,tot}^* = \dot{\omega}_{T,tot}/q_l^0$ for four different initial distances y^*.

The wall heat flux behavior is similar to the flux observed in the premixed flame case. The lower is y^*, the faster is the wall heat flux increase and the higher is its maximum value. Note that the influence of the initial distance is low during most part of the wall heat flux decrease phase, i.e. after $t^* = 800$. This is also true for the time evolution of the total reaction rate: except during a short period (from $t^* = 250$ to $t^* = 560$ approximately), the decrease in total reaction rate is the same for all y^*.

Fig. 10 and 11 show the maximum non-dimensional wall heat flux ϕ_Q and the characteristic time of the interaction t_Q^* as functions of the initial flame-wall distance y^*.

Figure 10 confirms the expected influence of the initial flame-wall distance on wall heat flux: the

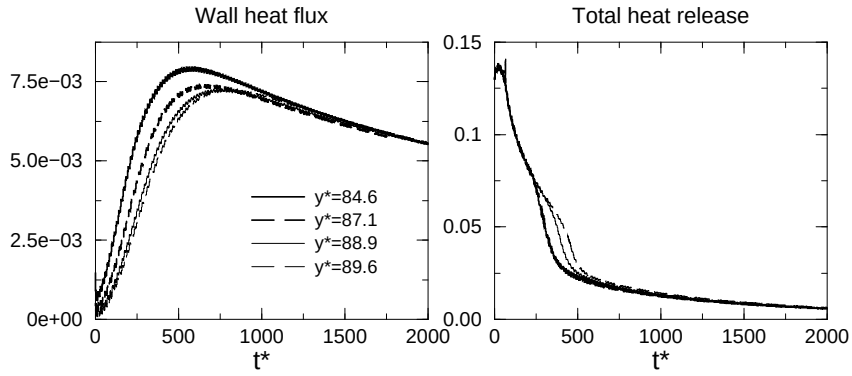

Figure 9: Non-dimensional wall heat flux and total heat release temporal evolution.

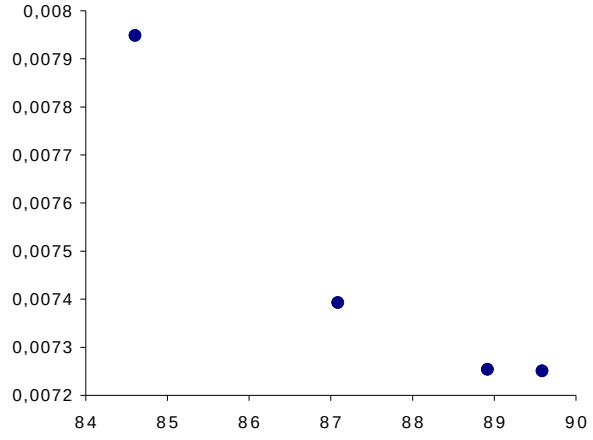

Figure 10: Non-dimensional maximum wall heat flux ϕ_Q versus initial flame-wall non-dimensional distance y^*.

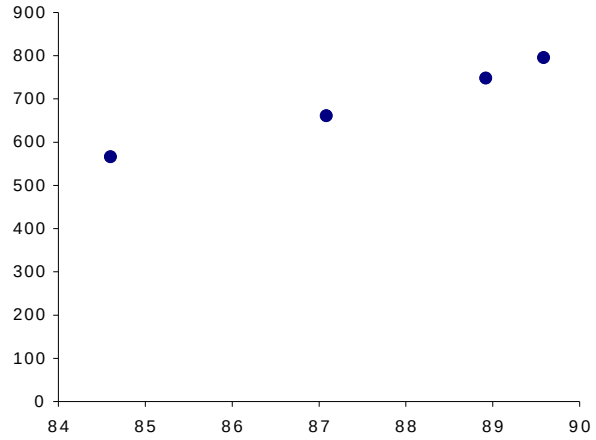

Figure 11: Non-dimensional characteristic time t^*_Q versus non-dimensional flame-wall distance y^*.

maximum heat flux is obtained for the minimum flame-wall initial distance, i.e. approximately half of the flame initial thickness. This corresponds to the flame placed closest to the wall without being perturbed (Fig. 6). The next step is then to vary the initial flame-wall thickness, and use the minimum flame-wall distance, in order to reach the maximum wall heat flux that can be obtained with this flame (Fig. 7). Initial values for the non-dimensional strain rate $\Lambda^* = \Lambda/\Lambda_Q$ where Λ_Q is the extinction strain rate, have been taken from 0.03 to $\approx$1. The corresponding initial flame-wall distances are shown on Fig. 12. At the critical extinction strain rate, the initial flame-wall distance is close to 17, i.e. 5 times lower than the initial distance of the lowest strain rate case ($\Lambda^* = 0.03$).

During the simulation, the flame first experiences a decrease of the strain rate as no straining velocity field is imposed, leading to an increase of flame temperature. Once the flame starts to significantly interact with the wall, the temperature decreases until extinction. This is illustrated in Fig. 13 where the maximum temperature has been plotted versus time for three different cases. However the maximum temperature reached during the interaction still remains a decreasing function of the strain rate, as shown on Fig. 14 where the maximum temperature is non-dimensonalized through $T_b^* = (T_b - T_w)/(T_{H2} - T_w)$. The maximum wall heat flux is then related to the ratio of two quantities

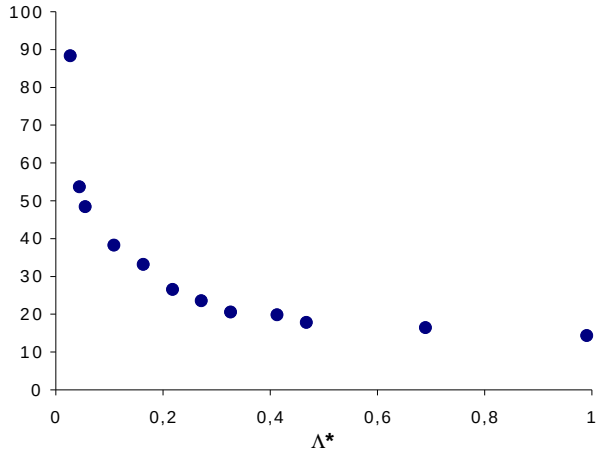

Figure 12: Initial flame-wall distance versus strain rate.

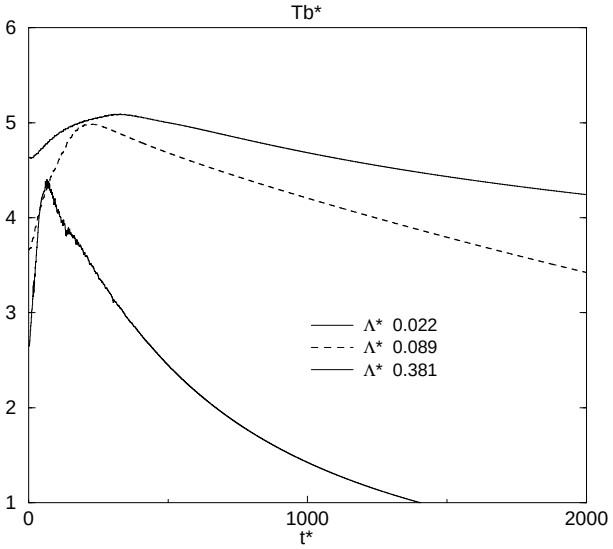

Figure 13: Time evolution of maximum temperature during interaction for different initial strain rates.

($(T_b - T_w)$ and y) both decreasing with the strain rate. Fig. 15 shows these two quantities as functions of one of the other. The distance y is a increasing function of the maximum temperature, with a low slope at lower temperatures (i.e. higher strain rates) and much sharper slope at higher temperatures (i.e. lower strain rates). Therefore we may expect an increasing maximum wall heat flux at lower strain rates and a lower increase, stagnation or even decrease when going to higher strain rates. This is observed on Fig. 17 showing the maximum reduced wall heat flux as a function of the strain rate. The maximum wall heat flux increases up to $\Lambda \approx 0.5$, reaching a maximum of 4.3 10^{-2}, then it decreases slowly until the extinction limit. We have obtained here the highest possible value for this H2/O2 flame in the HOQ configuration, as the flame can not exist closer to the wall.
It has been shown that, in simple chemistry calculations, the rough estimation of the maximum wall heat flux by the expression $\phi_Q^e = \lambda_w(T_b - T_w)/y$ gives reasonably good results ([18]). We have evaluated the validity of this estimation for complex chemistry flames by plotting the ratio ϕ_Q/ϕ_Q^e on

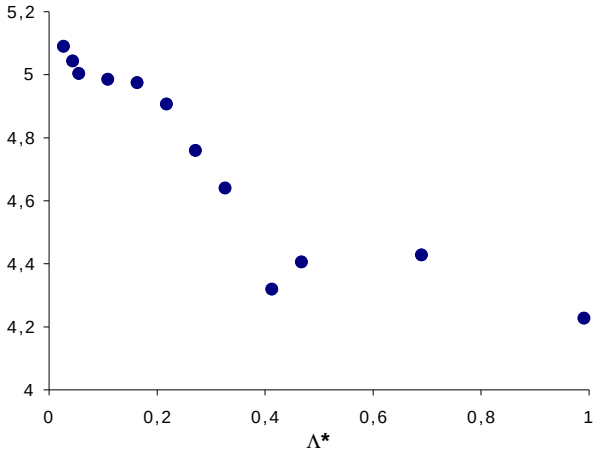

Figure 14: Maximum reduced temperature of the flame obtained for different strain rates.

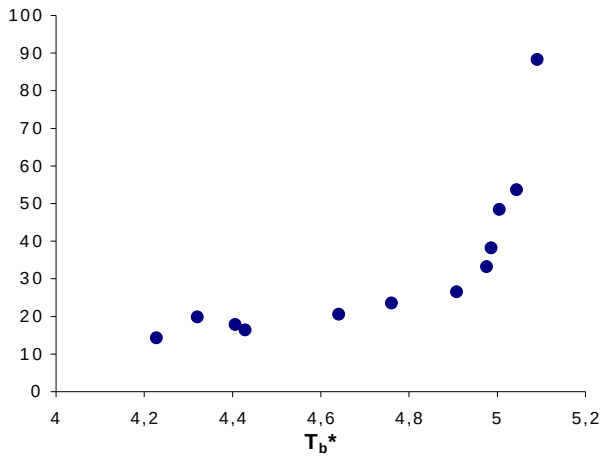

Figure 15: Intial flame-wall distance (based on maximum temperature) versus maximum temperature during the interaction with the wall.

Fig. 17. We find that the ratio remains close to a constant value, which is however different from 1. This almost constant ratio confirms that the maximum wall heat flux behaves like ϕ_Q^e, and shows that the mean gradient $(T_b - T_w)/y$ is about 3 times lower than the local temperature gradient at the wall. This is due to the complex composition of the mixture between the wall and the flame, responsible for a non-linear behavior of the temperature in this region. Nevertheless the approximation $\phi_Q \approx 3\lambda_w(T_b - T_w)/y$ is a good estimation for these flames and may be of great practical interest.

Compared to the premixed case, the maximum wall heat fluxes obtained for the diffusion flame are lower but, the interaction lasts much longer and more energy is delivered to the wall. The maximum wall heat flux obtained for the diffusion flame rises to approximately one third of the maximal value obtained for the premixed flame at 1 bar.

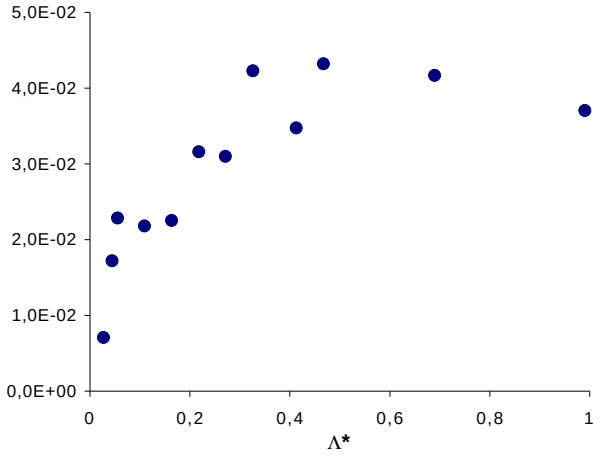

Figure 16: Non-dimensional maximum wall heat flux depending on the strain rate.

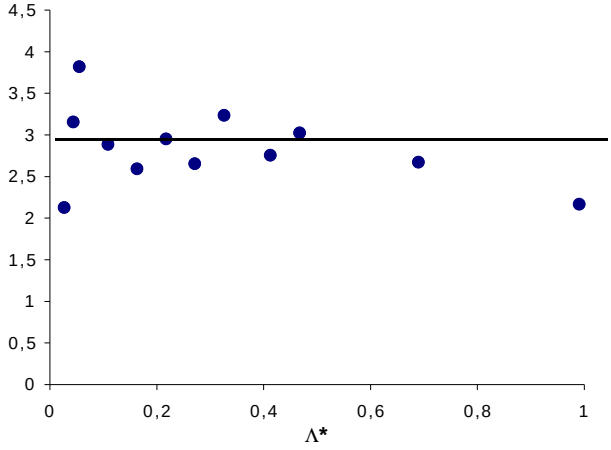

Figure 17: Ratio of the non-dimensional maximum wall heat flux and the estimated heat flux ϕ/ϕ_Q^e, depending on the strain rate.

4 Conclusions

Results of a laminar one-dimensional H2/O2 flame interacting with an inert constant temperature wall ($T_w = 750$K) have been reported for both the premixed and the diffusion flame. Calculations have been performed with detailed reaction mechanisms for a stoichiometric mixture at nearly atmospheric pressure. The flame quenching mechanisms for the premixed flame are approximately the same as for a hydrocarbon-air flame though the characteristic parameters of the interaction (ϕ_Q, $Pe_{F,Q}$, t_Q) differ notably. Results have shown the necessity of a good description of minor species HO_2 and H_2O_2. The low activation energy recombination reactions including these two species are responsible for about 30% of the wall heat flux.
Concerning the diffusion flame, the main result is that the maximum possible wall heat flux ϕ_Q appears to be one third of the flux obtained for a premixed flame. It is obtained at an intermediate strain rate, around one half of the critical extinction strain rate. For a given initial strain rate, ϕ_Q is roughly proportional to $\Delta T/y$ as shown in simple chemistry calculations.
Two important assumptions used in this study need further investigations: (i) the absence of catalytic reactions at the wall, and (ii) the equality $T_w = T_u$ which implies that there is no thermal boundary layer.

Acknowledgments

This work was supported by SNECMA-Moteurs, Division Moteurs-fusées and CNES (Centre National d'Etudes Spatiales). The support of IDRIS is also acknowledged for computing resources.

List of Figures

References

[1] I. Wichman and G. Bruneaux. *Combustion and Flame* 103:296-310 (1995).

[2] J. Jarosinski. *Comb. Sci. and Tech.* 12:81–116 (1986).

[3] Ezekoye O.A., Greif R., and Sawyer R.F. *Twenty-fourth Symposium (International) on Combustion*, The Combustion Institute, Pittsburgh, 1992, p. 1465.

[4] T. Poinsot, D. Haworth, and G. Bruneaux. *Combustion and Flame* 95:118–133 (1993).

[5] A. Delataillade, F. Dabireau, B. Cuenot, and T. Poinsot. *Proc. of the Combustion Institute* 29: (2002).

[6] T. Poinsot and D. Veynante. *Theoretical and numerical combustion.* R.T.Edwards, 2001.

[7] G. Bruneaux, K. Akselvoll, T. Poinsot, and J. Ferziger. *Combustion and Flame* 107:27–44 (1996).

[8] T. Alshaalan and C.J. Rutland. *Twenty-seventh Symposium (International) on Combustion*, The Combustion Institute, Pittsburgh, 1998, p. 793.

[9] Miller J.A., Mitchell R.E., Smooke M., and Kee R.J. *Nineteenth Symposium (International) on Combustion*, The Combustion Institute, Pittsburgh, 1982, p. 181.

[10] Kee R.J., Rupley F.M., and Miller J.A. *Chemkin-II: A Fortran Chemical Kinetics Package for the Analysis of Gas-Phase Chemical Kinetics.* Sandia National Laboratories Report No. SAND89-8009, 1989.

[11] Kee R.J., Warnatz J., and Miller J.A. *A fortran computer code package for the evaluation of gas phase viscosities, conductivities, and diffusion coefficients.* Sandia National Laboratories Report No. SAND83-8209, 1983.

[12] Kee R.J., Grcar J.F., Smooke M.D., and Miller J.A. *PREMIX: A fortran program for modeling steady laminar one-dimensional premixed flame.* Sandia National Laboratories Report No. SAND85-8240, 1985.

[13] T. Poinsot and S. Lele. *Jour. of Comput. Physics* 101:104–129 (1992).

[14] Vosen S.R., Greif R., and Westbrook C.K. *Twentieth Symposium (International) on Combustion*, The Combustion Institute, Pittsburgh, 1984, p. 76.

[15] Westbrook C.K., Adamczyk A.A., and Lavoie G.A. *Combustion and Flame* 40:81–99 (1981).

[16] Huang W.M., Vosen S.R., and Greif R. *Twenty-first Symposium (International) on Combustion*, The Combustion Institute, Pittsburgh, 1986, p. 1853.

[17] Popp P., Smooke M., and Baum M. *Twenty-sixth Symposium (International) on Combustion*, The Combustion Institute, Pittsburgh, 1996, p. 2693.

[18] T. Poinsot, C. Angelberger, B. Cuenot, and B. Bédat. CERFACS Report No. IR/CFD/98/66, 1998.